Pressure-enhanced superconducting transition in the inter-block-layer electron-transfer superconductor $BaTh_2Fe_4As_4(N_{0.7}O_{0.3})_2$

Pengfei Shan,[1,2] Pengtao Yang,[1,2] Yeting Shao,[3] Ziyi Liu,[1,2] Jun Hou,[1,2] Bosen Wang,[1,2] Yoshiya Uwatoko,[4] Guanghan Cao,[3] Jianping Sun,[1,2,*] and Jinguang Cheng[1,2]

[1]*Beijing National Laboratory for Condensed Matter Physics and Institute of Physics, Chinese Academy of Sciences, Beijing 100190, China*
[2]*School of Physical Sciences, University of Chinese Academy of Sciences, Beijing 100190, China*
[3]*Department of Physics, Zhejiang University, Hangzhou 310027, China*
[4]*Institute for Solid State Physics, University of Tokyo, Kashiwa, Chiba 277-8581, Japan*

(Received 28 August 2023; revised 14 November 2023; accepted 20 November 2023; published 7 December 2023)

The 12442-type hybrid structure compound $BaTh_2Fe_4As_4(N_{0.7}O_{0.3})_2$ is a recently synthesized inter-block-layer electron-transfer superconductor with separated double Fe_2As_2 layer and shows the superconducting transition at $T_c^{onset} \sim 30$ K and $T_c^{zero} \sim 20$ K. Here, we perform the resistivity measurements under various hydrostatic pressures up to ~12 GPa to track the evolution of its superconducting T_c and normal-state properties as a function of pressure. We found that $T_c(P)$ exhibits a nonmonotonic variation with pressure forming a dome-shaped superconducting phase, i.e., T_c^{onset} first increases quickly from ~30 K at ambient pressure to the optimal values of ~46 K at 2.6 GPa and then decreases gradually to ~23 K upon further increasing pressure to ~12 GPa. However, T_c^{zero} merely increases from ~21 K at ambient pressure to ~24 K at 2.6 GPa and then to ~12 K at ~12 GPa, leading to an obvious broadening of the superconducting transition at 2.6 GPa. Concomitant with the domed-shaped superconducting phase, the linear-temperature resistivity coefficient A_1 described by the empirical formula $\rho = \rho_0 + A_1 T + A_2 T^2$ also exhibits a similar dome-shaped structure, which may establish the positive correlation between T_c and A_1 as found in the unconventional high-T_c superconductors. Our high-pressure x-ray diffraction measurements rule out the occurrence of structural transition or a half-collapsed phase transition in the measured pressure range. Thus, our results indicate that the application of pressure may optimize the superconducting T_c by enhancing the inter-block-layer electron-transfer and/or the spin fluctuations in $BaTh_2Fe_4As_4(N_{0.7}O_{0.3})_2$.

DOI: 10.1103/PhysRevMaterials.7.124801

I. INTRODUCTION

The discovery of FeAs-based high-temperature superconductors has ignited excitement to explore more superconducting compounds holding the antifluoritelike Fe_2As_2-layer structural motif, which has led to the subsequent discovery of several families of Fe-based superconductors [1–7]. Following the block-layer-design approach, as shown in the superconductor $Ba_2Fe_2Ti_2As_4O$ with an intergrowth of $BaFe_2As_2$ and $BaTi_2As_2O$ [8], a series of bi-Fe_2As_2-layered 1144-type $MAeFe_4As_4$ and 12442-type $M(Ae/R)_2Fe_4As_4(F/O)_2$ superconductors were synthesized through the intergrowth between $ThCr_2Si_2$-type (122) and/or ZrCuSiAs-type (1111) FeAs-based parent compounds [9–12], where M = alkaline metal, Ae = alkaline earth metal, and R = rare-earth metal. Due to the heavily hole-doped characteristics in 122-type MFe_2As_2 such as KFe_2As_2 [2], the hybrid intergrowth superconducting compounds are intrinsically self-hole-doped with charge transfer between two constituent layers. According to the reported results, these hybrid bi-Fe_2As_2-layer intergrowth superconductors show the superconducting transition at $T_c \approx 28 - 37$ K [12–20]. In comparison with the single Fe_2As_2-layered superconductors, the unique asymmetric double Fe_2As_2 layers as well as the lattice mismatch and the bilayer thickness (i.e., the c/a ratio) make them more intricate, as shown in extensive studies [12,19]. Based on first-principles calculations, the multiband character is more complex than conventional iron-based superconductors [21,22]. In addition, quasi-two-dimensional electronic behavior and the nodal multigap structure have stimulated researchers to further explore the pairing states with the asymmetry of arsenic located at both sides of the Fe plane [23–25]. Thus, the pairing mechanisms related to the lattice/magnetism instabilities, spin fluctuations, and/or orbital degrees of freedom remain elusive for the observed unconventional superconductivity [23,25–27].

Recently, a series of electron-doped 12442-type hybrid-structure superconductors $BaTh_2Fe_4As_4(N_{1-x}O_x)_2$ was synthesized via an intergrowth between the 1111-type superconductor $ThFeAsN_{1-x}O_x$ and 122-type $BaFe_2As_2$ [28]. As indicated by the structural analysis, it is the shrinkage of the c axis and oxygen doping that enhances the Coulomb attractions and interlayer chemical bonding to stabilize the 12442 phase. For the conventional FeAs-based superconductors, the optimal superconducting T_c appears at $h_{As} = 1.38$ Å (the As height relative to the Fe plane) and $\alpha = 109.5°$ (the As–Fe–As bond angle) [29]. In contrast, these values in the optimal

*jpsun@iphy.ac.cn

doping $BaTh_2Fe_4As_4(N_{0.7}O_{0.3})_2$ samples are $h_{As} = 1.302$ and 1.343 Å and $\alpha = 113.7^\circ$ and 112.1° with inequivalent As sites, which are substantially lower than the optimal h_{As} and obviously larger than the α value in the single Fe_2As_2-layered superconductors [28], while for the hole-doped 12442-type bi-Fe_2As_2-layered superconductors, the deviations are strictly opposite with a larger h_{As} and smaller α values [17]. The Hall measurements of $BaTh_2Fe_4As_4(N_{0.7}O_{0.3})_2$ samples further confirm the electron-doping nature that is correlated with the interlayer charge transfer [28]. On the other hand, the transport measurements show that its normal-state resistivity $\rho(T)$ exhibits coherent Fermi-liquid behavior in a wide temperature range, which is noticeably contrary to the counterpart hole-doped 12442-type superconductors [12,16,17].

So far, several high-pressure studies have been performed on the 1144- and 12442-type hybrid superconductors [30–34]. First, a half-collapsed tetragonal phase was evidenced in $CaKFe_4As_4 \sim 4$ GPa, coinciding with the changes of the electronic properties and the disappearance of the bulk superconductivity [32]. In comparison, the collapsed tetragonal phase appears in $CaFe_2As_2$ at ~0.4 GPa [35,36]. For the Eu-based hybrid superconductors $EuRbFe_4As_4$ and $EuCsFe_4As_4$ that show the coexistence of superconductivity and robust Eu-spin ferromagnetism, the half-collapsed tetragonal phase transition was also confirmed at pressures $\sim 10 - 12$ GPa, and another fully collapsed tetragonal phase probably formed over ~20 GPa in $EuRbFe_4As_4$ [31]. Interestingly, a crossover from ferromagnetic superconductor ($T_c > T_m$) to superconducting ferromagnet ($T_m > T_c$) occurs in $EuRbFe_4As_4$ and $EuCsFe_4As_4$ at ~7 GPa, which is prior to the tetragonal to half-collapsed tetragonal phase transition, thus providing an ideal platform for further investigations among magnetism, superconductivity, and crystal structure [14,31,37], while in $KCa_2Fe_4As_4F_2$ and $RbGd_2Fe_4As_4O_2$, pressure drives the systems from non-Fermi-liquid to Fermi-liquid behavior, which may correlate with the reduction of electronic correlation and/or spin fluctuations, and no pressure-induced half-collapsed tetragonal phase occurs up to 15 GPa [33,34]. Thus, the strong interplay between lattice instability, spin fluctuations, and superconductivity still needs further exploration in these systems.

Given the substantially different lattice parameters, carrier types, and ground states in self-hole-doped and inter-block-layer electron-transfer 12442-type superconductors [17,28], here, we further performed high-pressure resistivity measurements to study the pressure effect on the superconducting T_c and the normal-state behaviors in $BaTh_2Fe_4As_4(N_{0.7}O_{0.3})_2$ under various pressures up to ~12 GPa. We found that the T_c values show a nonmonotonic evolution with pressures, which outlines a superconducting dome with the optimal $T_c^{onset} \sim 46$ K and $T_c^{zero} \sim 24$ K at 2.6 GPa with a sharp enhancement of the transition width to ~22 K. Moreover, the normal state of resistivity gradually evolves from Fermi-liquid to non-Fermi-liquid behavior at $P \geqslant 2.6$ GPa. Accompanying the crossover from Fermi-liquid to non-Fermi-liquid behavior, the highest superconducting T_c was achieved with an increase of the linear resistivity coefficient. Thus, our results indicate that the application of pressure may enhance the inter-block-layer electron-transfer and/or the spin fluctuations and then realize the optimal superconducting T_c with non-Fermi-liquid behavior.

II. EXPERIMENTAL DETAILS

The polycrystalline $BaTh_2Fe_4As_4(N_{0.7}O_{0.3})_2$ samples used in this paper were synthesized by a high-temperature solid-state-reaction method as described elsewhere [28]. The standard four-probe method was employed to measure the temperature dependence of resistivity $\rho(T)$ in a piston cylinder cell (PCC) up to 2 GPa and palm cubic anvil cell (CAC) up to 12 GPa. Here, we use Daphne 7373 oil in PCC and glycerol in CAC as the liquid pressure transmit medium (PTM) for all high-pressure measurements, which can maintain a good hydrostatic pressure. The pressure values inside the PCC and CAC were calibrated by observing the superconducting transition of lead (Pb) at low temperatures.

The high-pressure x-ray diffraction (HP-XRD) experiments were performed on the $BaTh_2Fe_4As_4(N_{0.7}O_{0.3})_2$ powder samples at room temperature in the 4W2 beamline of Beijing Synchrotron Radiation Facility (BSRF) by using monochromatic x-ray radiation of wavelength $\lambda = 0.6199$ Å. The pressure values of the symmetric diamond anvil cell (DAC) were determined by the ruby fluorescence method at room temperature. Methanol and ethanol with a 4:1 ratio was used as the PTM to ensure the hydrostatic pressure condition.

III. RESULTS AND DISCUSSIONS

Figure 1 shows the temperature dependence of resistivity $\rho(T)$ in the whole temperature range and the low-temperature range up to 11.7 GPa. As can be seen in Figs. 1(a) and 1(c), $\rho(T)$ exhibits the typical metallic behavior without a humplike feature at high temperatures which is always seen in the FeAs-based superconductors [12,16–18]. At ambient pressure, $\rho(T)$ follows a nearly quadratic temperature dependence from 100 K down to the superconducting transition $T_c^{onset} \sim 30$ K, as indicated by the dashed lines in Figs. 1(a) and 1(c). All the measured transport properties are in good agreement with previous reported data [28]. With increasing pressure to 11.7 GPa, the normal state of $\rho(T)$ decreases gradually, but the superconducting transition temperature T_c displays a nonmonotonic evolution, which can be seen more clearly in Figs. 1(b) and 1(d). Here, we define T_c^{onset} (up-pointing arrow) as the temperature where $\rho(T)$ starts to deviate from the extrapolated normal-state behavior and determine T_c^{zero} (down-pointing arrow) as the zero-resistivity temperature. At ambient pressure, the superconducting transition is quite broad with $T_c^{onset} \sim 30$ K and $T_c^{zero} \sim 21$ K. When we apply the pressure gradually in PCC, both T_c^{onset} and T_c^{zero} increase and reach $T_c^{onset} \sim 35$ K and $T_c^{zero} \sim 23$ K at 1.99 GPa, Fig. 1(b). At 2.6 GPa in CAC, T_c^{onset} was further enhanced to an optimal value of ~46 K. Upon further increasing pressure to 11.7 GPa, T_c^{onset} is gradually suppressed to ~22 K, but T_c^{zero} does not change too much in the measured pressure range. It was merely enhanced from ~21 K at ambient pressure to ~24 K at 2.6 GPa and then was finally suppressed to ~12 K at 11.7 GPa.

Based on the above high-pressure resistivity measurements, the pressure dependences of T_c^{onset} and T_c^{zero} for two

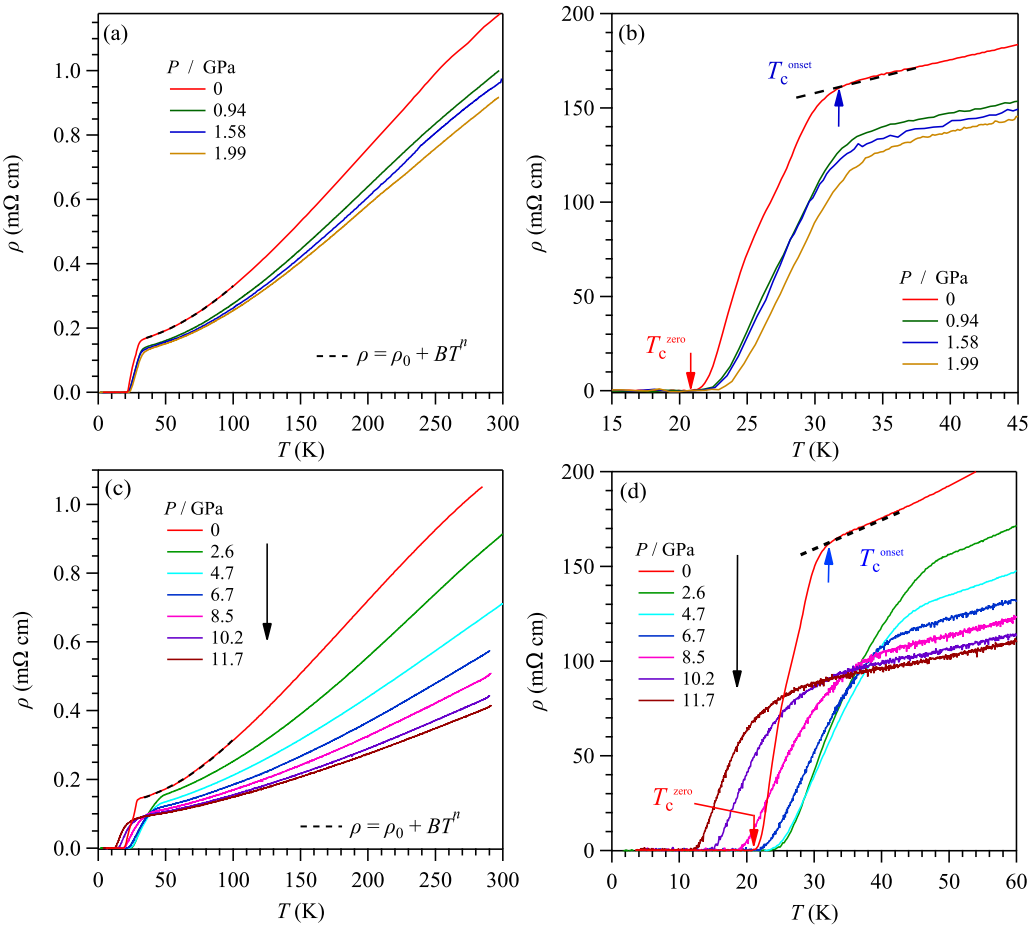

FIG. 1. (a) and (c) Temperature-dependent resistivity $\rho(T)$ curves in the whole temperature range under various pressures up to 1.99 and 11.7 GPa. (b) and (d) The resistivity $\rho(T)$ curves < 45 and 60 K showing the variation of the superconducting transition with pressure. The dashed lines in (a) and (c) are the fitting curve by using $\rho = \rho_0 + AT^n < 100$ K. The superconducting transition in (b) and (d) are marked by bule and red arrows.

different samples are summarized in Fig. 2(a), which explicitly reveals the asymmetric superconducting dome. The superconducting transition T_c^{onset} first shows a sharp increase from ~30 K at ambient pressure to the optimal value ~46 K at 2.6 GPa, whereas T_c^{zero} only increases by ~3 K, resulting in a very broad superconducting transition width ΔT_c ($\equiv T_c^{onset} - T_c^{zero}$) ~22 K at $P_c = 2.6$ GPa. Above 2.6 GPa, ΔT_c exhibits a linear decrease with a rate ~1.3 K/GPa, Fig. 2(b). Here, we should mention that the dramatic enhancement of T_c^{onset} and superconducting transition width may originate from pressure-enhanced superconducting fluctuations. Therefore, T_c^{zero} is closer to the bulk superconductivity. To further understand the observed pressure effect on the superconducting T_c of the electron-doped 12442-type compound $BaTh_2Fe_4As_4(N_{0.7}O_{0.3})_2$ would help us to further understand the superconducting mechanism of these hybrid structure Fe-based superconductors. For this purpose, we analyzed the normal state $\rho(T)$ to further elucidate the inherent correlations with the evolution of T_c^{zero} under high pressures. As displayed in Figs. 1(a) and 1(c), the $\rho(T)$ data were fitted by $\rho(T) = \rho_0 + BT^n$ for $T < 100$ K, where ρ_0 is the residual resistivity, and n is the resistivity exponent. The fitting results are shown in Fig. 2(b). Here, we can see clearly that the resistivity exhibits Fermi-liquid behavior at $P < 2$ GPa with $n \approx 2$, which evolves to $n \approx 1.6$ at $P \geqslant 2.6$ GPa. Such an evolution demonstrates that pressure can drive the system from Fermi-liquid to non-Fermi-liquid behavior, accompanying the emergence of the optimal superconducting transition T_c^{zero}. It is noteworthy that the observed $\rho(T) \sim T^{1.6}$ in $BaTh_2Fe_4As_4(N_{0.7}O_{0.3})_2$ is reminiscent of cuprates at the verge of the superconducting dome in the overdoped $La_{2-x}Sr_xCuO_4$ and $La_{2-x}Ce_xCuO_4$, and it has been attributed to the quantum criticality [38,39].

Thus, the above observations indicate that the pressure-enhanced superconductivity in $BaTh_2Fe_4As_4(N_{0.7}O_{0.3})_2$ near $P_c \sim 2.6$ GPa may be correlated with enhanced quantum critical fluctuations. In this sense, we further employ the empirical formula $\rho = \rho_0 + A_1 T + A_2 T^2$ to fit the resistivity data under high pressures, which has been used to establish a relation between the temperature coefficient and the evolution of T_c in a wide range of chemical doping or under high pressures in Fe-based superconductors and cuprates [38–41]. All the fitting parameters were obtained from Figs. 3(a) and 3(b) and summarized in Figs. 3(c)–3(e). Here, the linear term $A_1 T$ has been interpreted as the electron correlations and/or enhanced scattering of the critical fluctuations near the quantum critical region, whereas the $A_2 T^2$ term is described as Fermi-liquid behavior, and the divergence of the temperature coefficient is always typified as a signature of quantum

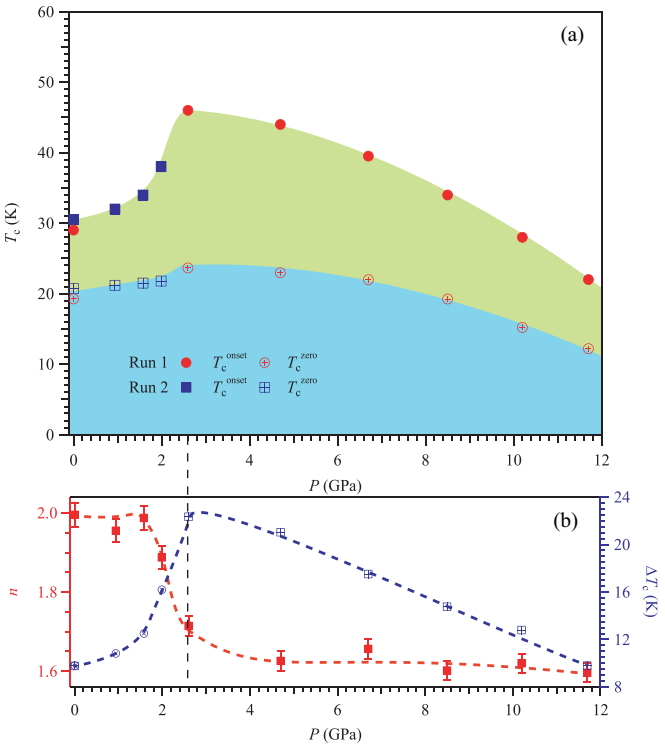

FIG. 2. (a) Pressure dependence of the superconducting transition temperatures T_c^{onset} and T_c^{zero} of $BaTh_2Fe_4As_4(N_{0.7}O_{0.3})_2$ for two samples in Runs 1 and 2. (b) Pressure dependence of the resistivity exponent n by using $\rho = \rho_0 + BT^n < 100$ K and the superconducting transition width ΔT_c.

critical point. In Fig. 3(c), ρ_0 decreases monotonically in the whole pressure range and displays a slope change above the critical pressure of 2.6 GPa. According to other reports, the smooth decrease of ρ_0 can rule out the formation of a collapsed tetragonal structure [32,42,43], which is consistent with our high-pressure structural study as shown below. Due to the polycrystalline character, we use the relative changes of $A_1(P)/A_1(AP)$ and $A_2(P)/A_2(AP)$ to make our results more reasonable, where AP and P represent the data at ambient pressure and high pressures, as shown in Figs. 3(d) and 3(e). With increasing pressure gradually, $A_1(P)/A_1(AP)$ increases quickly by one order of magnitude from ambient to 2.6 GPa, which coincides with the enhancement of T_c^{zero}. Above 2.6 GPa, $A_1(P)/A_1(AP)$ exhibits a slow decrease upon further increasing pressure to 11.7 GPa. Interestingly, the shape of $A_1(P)/A_1(AP)$ reproduces the superconducting dome of $T_c^{zero}(P)$ under high pressure, and the similar evolution of A_1 and T_c implies that the T-linear term has an intimated correlation with the superconducting phase. Therefore, the electron scattering and pairing are most likely associated with critical spin fluctuations [38,39]. Meanwhile, $A_2(P)/A_2(AP)$ first declines dramatically with increasing pressure to 2.6 GPa and then decreases at a slow rate at $P > 2.6$ GPa, as presented in Fig. 3(e). These results indicate that the linear-temperature term A_1T is strongly coupled with the superconducting T_c^{zero}, while the quadratic term shows a weak correlation with the superconducting phase. The crossover from Fermi-liquid to non-Fermi-liquid behavior at the critical pressure mimics an extended quantum critical boundary coinciding with the enhancement of T_c^{zero} in this paper. Therefore, the evolution of the normal state under high pressures in the inter-block-layer electron-transfer 12442-type hybrid superconductor is exactly opposite to the self-hole doped 12442-type superconductors which show a pressure-drive crossover from non-Fermi-liquid to Fermi-liquid behavior [33,34]. However, we should note that the studied polycrystalline samples might weaken the above quantitative analysis, and more efforts should be made on single-crystal samples to obtain rigorous conclusions when they become available.

To further reveal the structure information of $BaTh_2Fe_4As_4(N_{0.7}O_{0.3})_2$ under high pressures, we preformed XRD measurements up to 12.5 GPa at room temperature. As displayed in Fig. 4(a), no diffraction peaks split, and no extra diffraction peaks appear upon increasing pressure to 12.5 GPa, thus ruling out any structural phase transition in the measured pressure range up to 13 GPa. Here, we use the LeBail fit to analyze these XRD data in a tetragonal unit cell and extract the pressure dependences of lattice parameters a, c and volume V, as shown in Figs. 4(b) and 4(c). For the double-Fe_2As_2-layered structure with longer c, we can see that the c axis is more easily compressed than the a axis. For example, the a axis is only shortened by ∼2.1%, whereas the c axis is reduced by ∼7% up to 12.5 GPa. On the other hand, the volume $V(P)$ shows a continuous decrease and can be fitted well with the Birch-Murnaghan (BM) equation, yielding the bulk modulus $B_0 = 78.9$ GPa and $V_0 = 475.1$ Å^3. Moreover, the ratio of c/a exhibits a nearly linear decrease from 7.48 at ambient pressure to 7.11 at 12.5 GPa. The continuous decrease of the volume and the nearly linear decrease of c/a further exclude the occurrence of the collapsed phase or half-collapsed phase.

By employing the high-pressure resistivity measurements, we have tracked the evolutions of the normal state and the superconducting transition in $BaTh_2Fe_4As_4(N_{0.7}O_{0.3})_2$ and constructed a dome-shaped superconducting phase diagram as shown in Fig. 2. Under high pressures, T_c^{onset} and T_c^{zero} first show increases to ∼46 and ∼24 K at 2.6 GPa with the normal state changing from Fermi-liquid to non-Fermi-liquid behavior and then decreases gradually to ∼23 and ∼12 K with further increasing pressure to 11.7 GPa. Moreover, the superconducting transition width ΔT_c also exhibits a rapid rise from ∼9 K at ambient pressure to ∼22 K at 2.6 GPa and then shows a linear decrease to ∼10 K at 11.7 GPa. Here, it should be noted that the broadening of the superconducting transition is not induced by the inhomogeneous of pressure since ΔT_c exhibits a continuous decrease at higher pressures $>$ 2.6 GPa. Therefore, the nonmonotonic evolution of ΔT_c can be explained by the onset of superconducting transition coming from the pressure enhanced superconducting fluctuations, while in the 12442-type self-hole-doped $KCa_2Fe_4As_4F_2$ and $RbGd_2Fe_4As_4O_2$ polycrystals, high-pressure monotonically suppresses the superconducting transition [33,34]. For the normal state, the hole-doped and electron-doped 12442-type superconductors exhibit completely different evolutions. At ambient pressure, $KCa_2Fe_4As_4F_2$ and $RbGd_2Fe_4As_4O_2$ show non-Fermi-liquid behavior, and high pressure drives these systems to the conventional Fermi-liquid behavior with the reduction of T_c [33,34]. However, the $BaTh_2Fe_4As_4(N_{0.7}O_{0.3})_2$

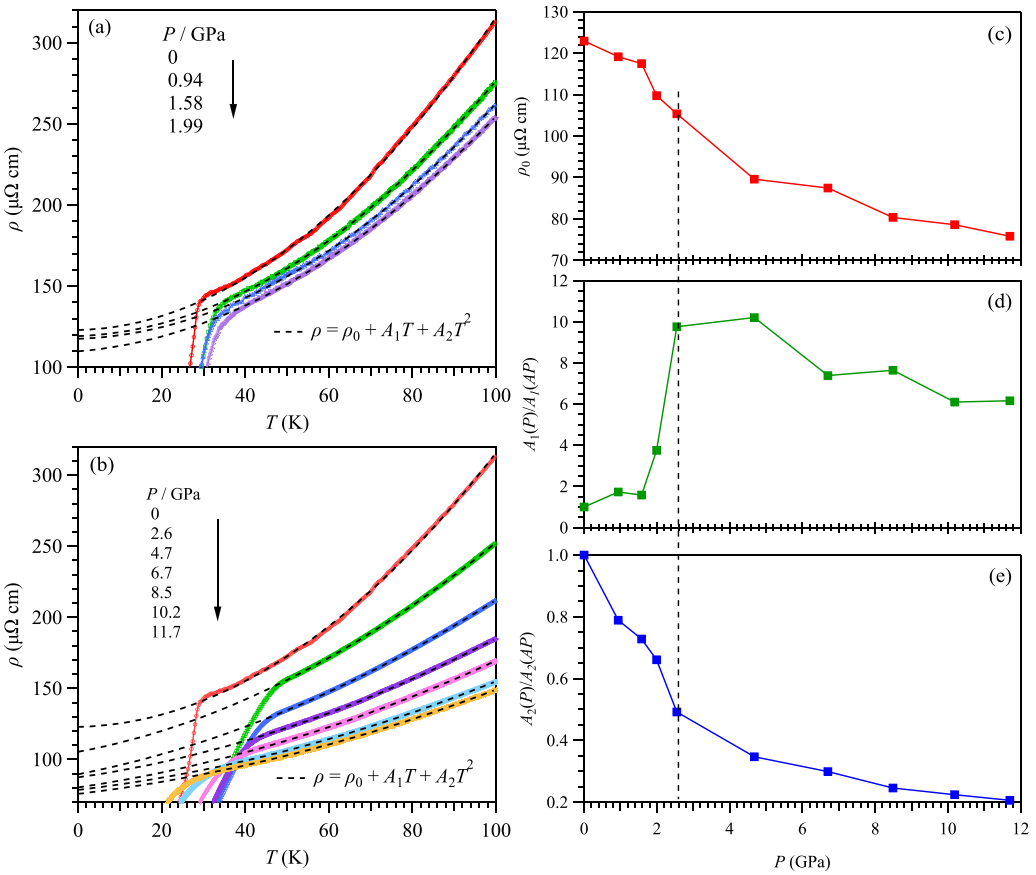

FIG. 3. (a) and (b) Temperature dependence of resistivity $\rho(T)$ at $T < 100$ K under various pressures up to 1.99 and 11.7 GPa. A simple fitting by the formula $\rho(T) = \rho_0 + A_1 T + A_2 T^2$ is applied to fit the normal state of $\rho(T)$, as shown by the dashed line. Pressure dependence of related fitting parameters: (c) the residual resistivity ρ_0, (d) the $A_1(P)/A_1(AP)$ values, and (e) $A_2(P)/A_2(AP)$ values, where AP and P represent the data at ambient pressure and high pressures. The dashed line indicates the critical pressure 2.6 GPa.

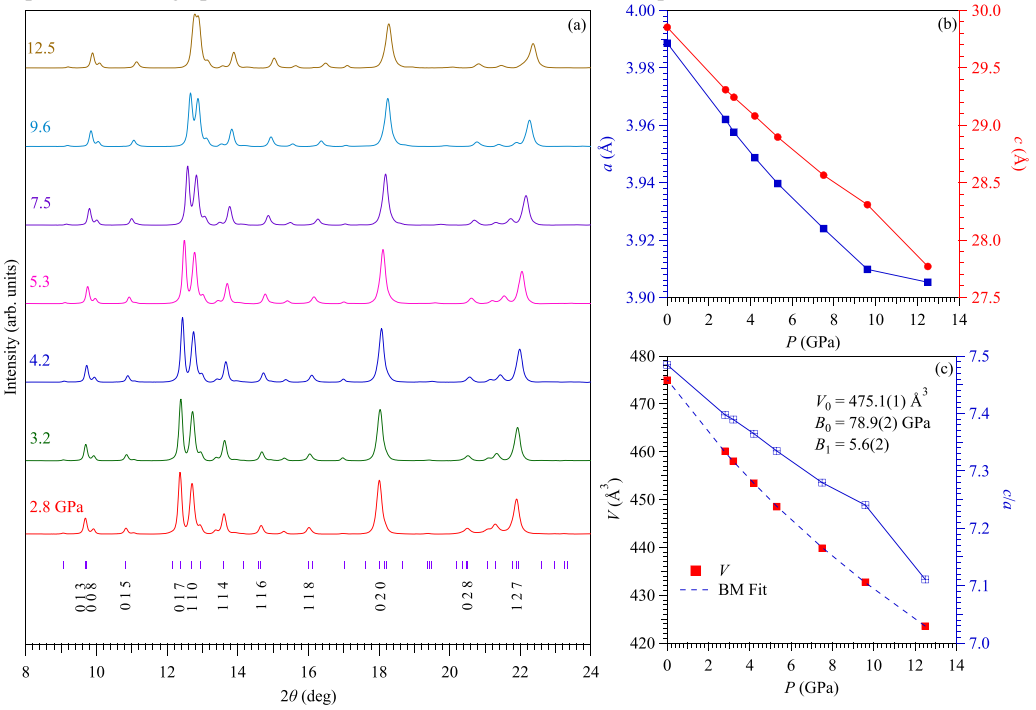

FIG. 4. (a) High-pressure x-ray diffraction (XRD) patterns of $BaTh_2Fe_4As_4(N_{0.7}O_{0.3})_2$ at room temperature under various pressures up to 12.5 GPa. (b) and (c) Pressure dependences of lattice parameters a, c, and volume V. The solid line in (c) represents the fitting result of the Birch-Murnaghan equation.

samples display Fermi-liquid behavior at ambient pressure, and high pressure changes its normal state to non-Fermi-liquid behavior with an increase of T_c. Our study suggests that the superconducting transition may have direct correlation with the evolution of the normal state in $BaTh_2Fe_4As_4(N_{0.7}O_{0.3})_2$.

As reported in the FeAs-based superconductors, the dome-shaped $T_c(x, P)$ phase diagram with optimal superconducting T_c usually emerges near an antiferromagnetic quantum critical point, and the resistivity usually exhibits non-Fermi-liquid behavior [5,44,45]. For $BaTh_2Fe_4As_4(N_{0.7}O_{0.3})_2$, its doping level is ∼0.15 electrons per Fe, and it is likely located in the overdoped region as seen in the electron-doped $Ba(Fe_{1-x}Co_x)_2As_2$ or $Ba(Fe_{1-x}Ni_x)_2As_2$, where Fermi-liquid behavior dominates the normal state [46–49]. Under high pressures, the electron-transfer between different constituent layers may be enhanced and thus improves the electron scattering between different Fermi surfaces or spin fluctuations due to the smaller h_{As} values. Therefore, its normal state is gradually changed with increasing pressures. Our study further indicates that the sharp increase of $A_1(P)/A_1(AP)$ at $P_c = 2.6$ GPa may have correlations to the enhancement of spin fluctuations which is usually observed in other FeAs-based superconductors [25,50,51]. At this critical pressure 2.6 GPa, the superconducting transition was greatly enhanced with the increase of $A_1(P)/A_1(AP)$ values, which has been seen in similar evolutions in the cuprates [38,39,52]. On the contrary, the hole-doped 12442-type superconductors may locate exactly near the critical point at ambient pressure, as seen in hole-doped $Ba_{1-x}K_xFe_2As_2$ [53]. The application of high pressure drives the system away from the critical point, accompanying the reduction of $A_1(P)/A_1(AP)$ and superconducting T_c.

Finally, it is instructive to compare the results of 12442-type $BaTh_2Fe_4As_4(N_{0.7}O_{0.3})_2$ with those of 1111-type ThFeAsN, which has been well studied recently [30,54–56]. As indicated by the nuclear magnetic resonance and muon-spin rotation measurements on ThFeAsN, the reduction of T_c is accompanied with the simultaneous suppression of antiferromagnetic spin fluctuations and a subtle modification of band structure [54]. Moreover, the high-pressure XRD measurements further reveal that the evolutions of T_c with reduction of the anion height or increase of bond angle follows the universal law of most FeAs-based superconductors [30]. However, $BaTh_2Fe_4As_4(N_{0.7}O_{0.3})_2$ deviates the optimal structure values and shows the smaller anion height and larger bond angle, which may rationalize the observed relatively low T_c of this system. Under high pressure, it violates this universal trend that its superconducting T_c^{onset} and T_c^{zero} first show an enhancement with decreasing the anion height or increasing the bond angle. This may correlate with the inter-block-layer charge transfer character that the shrinkage of the c axis under high pressure enhances the spin fluctuations and/or the charge transfer to the Fe_2As_2 layer and increases the superconducting T_c^{onset} and T_c^{zero} at $P < 2.6$ GPa. Here, no half-collapsed tetragonal phase transition was observed in the measured pressure range, and it is consistent with hole-doped 12442-type superconductors and ThFeAsN [30,33,34]. To further understand the evolutions of superconducting properties in $BaTh_2Fe_4As_4(N_{0.7}O_{0.3})_2$, more experiments are needed to reveal the electronic band structures and spin dynamics.

IV. CONCLUSIONS

In summary, we have performed high-pressure measurements on the recently synthesized 12442-type inter-block-layer electron-transfer superconductor $BaTh_2Fe_4As_4(N_{0.7}O_{0.3})_2$. It is found that the superconducting T_c under high pressure exhibits a nonmonotonic evolution, which first shows an increase from $T_c^{onset} \sim 30$ K and $T_c^{zero} \sim 21$ K at ambient pressure to the optimal values ∼46 and ∼24 K at 2.6 GPa and then decreases to ∼23 and ∼12 K at 11.7 GPa, outlining a dome-shaped superconducting phase. High-pressure XRD measurements rule out the occurrence of structural phase transition to the half-collapsed phase in the measured pressure range. In addition, the normal-state $\rho(T)$ at low temperatures gradually evolves from Fermi-liquid behavior at ambient pressure to non-Fermi-liquid behavior at $P \geqslant 2.6$ GPa, accompanied with a sharp increase of linear resistivity coefficient by about one order of magnitude compared with the value at ambient pressure. Thus, our results indicate that the enhancement of superconducting T_c^{zero} should have intimated correlations with enhanced spin fluctuations, which is consistent with the situation in cuprates that the linear-temperature term is strongly coupled with T_c.

ACKNOWLEDGMENTS

This paper is supported by the National Key R&D Program of China (No. 2022YFA1403900 and No. 2021YFA1400200), the National Natural Science Foundation of China (No. 12025408, No. 11921004, No. 11888101, No. 11834016, and No. 12174424), the Beijing Natural Science Foundation (No. Z190008), the CAS Project for Young Scientists in Basic Research (No. 2022YSBR-048), the Strategic Priority Research Program of the Chinese Academy of Sciences (No. XDB25000000 and No. XDB33000000), and the Youth Innovation Promotion Association of CAS (No. 2023007). Y.U. acknowledges the support from JSPS KAKENHI (No. JP19H00648). Z.L. acknowledges support from the China Postdoctoral Science Foundation (No. 2022M723354 and No. 2023T160676). The high-pressure XRD data were collected in the 4W2 beamline of Beijing Synchrotron Radiation Facility (BSRF).

[1] Y. Kamihara, T. Watanabe, M. Hirano, and H. Hosono, Iron-based layered superconductor $La[O_{1-x}F_x]FeAs$ ($x = 0.05 - 0.12$) with $T_c = 26$ K, J. Am. Chem. Soc. **130**, 3296 (2008).

[2] M. Rotter, M. Tegel, and D. Johrendt, Superconductivity at 38 K in the iron arsenide $(Ba_{1-x}K_x)Fe_2As_2$, Phys. Rev. Lett. **101**, 107006 (2008).

[3] X. C. Wang, Q. Q. Liu, Y. X. Lv, W. B. Gao, L. X. Yang, R. C. Yu, F. Y. Li, and C. Q. Jin, The superconductivity at 18 K in LiFeAs system, Solid State Commun. **148**, 538 (2008).

[4] J. G. Guo, S. F. Jin, G. Wang, S. C. Wang, K. X. Zhu, T. T. Zhou, M. He, and X. L. Chen, Superconductivity in the iron selenide $K_xFe_2Se_2$ ($0 \leqslant x \leqslant 1.0$), Phys. Rev. B **82**, 180520(R) (2010).

[5] G. R. Stewart, Superconductivity in iron compounds, Rev. Mod. Phys. **83**, 1589 (2011).

[6] F. C. Hsu, J. Y. Luo, K. W. Yeh, T. K. Chen, T. W. Huang, P. M. Wu, Y. C. Lee, Y. L. Huang, Y. Y. Chu, D. C. Yan *et al.*, Superconductivity in the PbO-type structure alpha-FeSe, Proc. Natl. Acad. Sci. USA **105**, 14262 (2008).

[7] J. H. Tapp, Z. J. Tang, B. Lv, K. Sasmal, B. Lorenz, P. C. W. Chu, and A. M. Guloy, LiFeAs: An intrinsic FeAs-based superconductor with $T_c = 18$ K, Phys. Rev. B **78**, 060505(R) (2008).

[8] Y. L. Sun, H. Jiang, H. F. Zhai, J. K. Bao, W. H. Jiao, Q. Tao, C. Shen, Y. Y. W. Zeng, Z. A. Xu, and G.-H. Cao, $Ba_2Ti_2Fe_2As_4O$: A new superconductor containing Fe_2As_2 layers and Ti_2O sheets, J. Am. Chem. Soc. **134**, 12893 (2012).

[9] A. Iyo, K. Kawashima, T. Kinjo, T. Nishio, S. Ishida, H. Fujihisa, Y. Gotoh, K. Kihou, H. Eisaki, and Y. Yoshida, New-structure-type Fe-based superconductors: $CaAFe_4As_4$ (A = K, Rb, Cs) and $SrAFe_4As_4$ (A = Rb, Cs), J. Am. Chem. Soc. **138**, 3410 (2016).

[10] A. Iyo, K. Kawashima, S. Ishida, H. Fujihisa, Y. Gotoh, H. Eisaki, and Y. Yoshida, Superconductivity in a new 1144-type family of (La,Na)AFe_4As_4 (A = Rb or Cs), J. Phys. Chem. Lett **9**, 868 (2018).

[11] J. K. Bao, K. Willa, M. P. Smylie, H. J. Chen, U. Welp, D. Y. Chung, and M. G. Kanatzidis, Single crystal growth and study of the ferromagnetic superconductor $RbEuFe_4As_4$, Cryst. Growth Des. **18**, 3517 (2018).

[12] Z. C. Wang, C. Y. He, S. Q. Wu, Z. T. Tang, Y. Liu, A. Ablimit, C. M. Feng, and G. H. Cao, Superconductivity in $KCa_2Fe_4As_4F_2$ with separate double Fe_2As_2 layers, J. Am. Chem. Soc. **138**, 7856 (2016).

[13] Y. Liu, Y. B. Liu, Q. Chen, Z. T. Tang, W. H. Jiao, Q. Tao, Z. A. Xu, and G.-H. Cao, A new ferromagnetic superconductor: $CsEuFe_4As_4$, Sci. Bull. **61**, 1213 (2016).

[14] Y. Liu, Y. B. Liu, Z. T. Tang, H. Jiang, Z. C. Wang, A. Ablimit, W. H. Jiao, Q. Tao, C. M. Feng, Z. A. Xu *et al.*, Superconductivity and ferromagnetism in hole-doped $RbEuFe_4As_4$, Phys. Rev. B **93**, 214503 (2016).

[15] C. Wang, Z. C. Wang, Y. X. Mei, Y. K. Li, L. Li, Z. T. Tang, Y. Liu, P. Zhang, H. F. Zhai, Z. A. Xu *et al.*, A new ZrCuSiAs-type superconductor: ThFeAsN, J. Am. Chem. Soc. **138**, 2170 (2016).

[16] Z. C. Wang, C. Y. He, Z. T. Tang, S. Q. Wu, and G.-H. Cao, Crystal structure and superconductivity at about 30 K in $ACa_2Fe_4As_4F_2$ (A = Rb, Cs), Sci. China Mater. **60**, 83 (2016).

[17] Z. C. Wang, C. Y. He, S. Q. Wu, Z. T. Tang, Y. Liu, A. Ablimit, Q. Tao, C. M. Feng, Z. A. Xu, and G. H. Cao, Superconductivity at 35 K by self doping in $RbGd_2Fe_4As_4O_2$, J. Phys. Condens. Matter **29**, 11LT01 (2017).

[18] Z. C. Wang, C. Y. He, S. Q. Wu, Z. T. Tang, Y. Liu, and G.-H. Cao, Synthesis, crystal structure and superconductivity in $RbLn_2Fe_4As_4O_2$ (Ln = Sm, Tb, Dy, and Ho), Chem. Mater. **29**, 1805 (2017).

[19] S. Q. Wu, Z. C. Wang, C. Y. He, Z. T. Tang, Y. Liu, and G. H. Cao, Superconductivity at 33–37 K in $ALn_2Fe_4As_4O_2$ (A = K and Cs; Ln = lanthanides), Phys. Rev. Mater. **1**, 044804 (2017).

[20] B. Z. Li, Z. C. Wang, J. L. Wang, F. X. Zhang, D. Z. Wang, F. Y. Zhang, Y. P. Sun, Q. Jing, H. F. Zhang, S. G. Tan *et al.*, Peculiar phase diagram with isolated superconducting regions in $ThFeAsN_{1-x}O_x$, J. Phys.: Condens. Matter **30**, 255602 (2018).

[21] Z. W. Wang, G. T. Wang, and X. Tian, Electronic structure and magnetism of $RbGd_2Fe_4As_4O_2$, J. Alloy. Compd. **708**, 392 (2017).

[22] D. X. Mou, T. Kong, W. R. Meier, F. Lochner, L. L. Wang, Q. S. Lin, Y. Wu, S. L. Bud'ko, I. Eremin, D. D. Johnson *et al.*, Enhancement of the superconducting gap by nesting in $CaKFe_4As_4$: A new high temperature superconductor, Phys. Rev. Lett. **117**, 277001 (2016).

[23] F. K. K. Kirschner, D. T. Adroja, Z. C. Wang, F. Lang, M. Smidman, P. J. Baker, G. H. Cao, and S. J. Blundell, Two-gap superconductivity with line nodes in $CsCa_2Fe_4As_4F_2$, Phys. Rev. B **97**, 060506(R) (2018).

[24] M. Smidman, F. K. K. Kirschner, D. T. Adroja, A. D. Hillier, F. Lang, Z. C. Wang, G. H. Cao, and S. J. Blundell, Nodal multigap superconductivity in $KCa_2Fe_4As_4F_2$, Phys. Rev. B **97**, 060509(R) (2018).

[25] K. Cho, A. Fente, S. Teknowijoyo, M. A. Tanatar, K. R. Joshi, N. M. Nusran, T. Kong, W. R. Meier, U. Kaluarachchi, I. Guillamon *et al.*, Nodeless multiband superconductivity in stoichiometric single-crystalline $CaKFe_4As_4$, Phys. Rev. B **95**, 100502(R) (2017).

[26] A. Fente, W. R. Meier, T. Kong, V. G. Kogan, S. L. Bud'ko, P. C. Canfield, I. Guillamón, and H. Suderow, Influence of multiband sign-changing superconductivity on vortex cores and vortex pinning in stoichiometric high-T_c $CaKFe_4As_4$, Phys. Rev. B **97**, 134501 (2018).

[27] Y. Li, Z. C. Wang, G. H. Cao, J. M. Zhang, B. Zhang, T. Wang, H. Pang, F. S. Li, and Z. W. Li, Mössbauer spectroscopy study of magnetic fluctuations in superconducting $RbGd_2Fe_4As_4O_2$, Phys. C: Supercond. Appl. **548**, 21 (2018).

[28] Y. T. Shao, Z. C. Wang, B. Z. Li, S. Q. Wu, J. F. Wu, Z. Ren, S. W. Qiu, C. Rao, C. Wang, and G.-H. Cao, $BaTh_2Fe_4As_4(N_{0.7}O_{0.3})_2$: An iron-based superconductor stabilized by inter-block-layer charge transfer, Sci. China Mater. **62**, 1357 (2019).

[29] X. G. Luo and X. H. Chen, Crystal structure and phase diagrams of iron-based superconductors, Sci. China Mater. **58**, 77 (2015).

[30] H. H. Wang, J. Guo, Y. T. Shao, C. Wang, S. Cai, Z. Wang, X. D. Li, Y. C. Li, G.-H. Cao, and L. L. Sun, Pressure effects on superconductivity and structural parameters of ThFeAsN, EPL **123**, 67004 (2018).

[31] D. E. Jackson, D. VanGennep, W. Bi, D. Z. Zhang, P. Materne, Y. Liu, G. H. Cao, S. T. Weir, Y. K. Vohra, and J. J. Hamlin, Superconducting and magnetic phase diagram of $RbEuFe_4As_4$ and $CsEuFe_4As_4$ at high pressure, Phys. Rev. B **98**, 014518 (2018).

[32] U. S. Kaluarachchi, V. Taufour, A. Sapkota, V. Borisov, T. Kong, W. R. Meier, K. Kothapalli, B. G. Ueland, A. Kreyssig, R. Valentí *et al.*, Pressure-induced half-collapsed-tetragonal phase in $CaKFe_4As_4$, Phys. Rev. B **96**, 140501(R) (2017).

[33] J. P. Sun, Z. C. Wang, Z. Y. Liu, S. X. Xu, T. Eto, Y. Sui, B. S. Wang, Y. Uwatoko, G.-H. Cao, and J.-G. Cheng, Effect of pressure on the self-hole-doped superconductor $RbGd_2Fe_4As_4O_2$, J. Phys.: Condens. Matter **31**, 044001 (2019).

[34] B. S. Wang, Z. C. Wang, K. Ishigaki, K. Matsubayashi, T. Eto, J. P. Sun, J.-G. Cheng, G.-H. Cao, and Y.

Uwatoko, Pressure-induced enhancement of superconductivity and quantum criticality in the 12442-type hybrid-structure superconductor $KCa_2Fe_4As_4F_2$, Phys. Rev. B **99**, 014501 (2019).

[35] A. Kreyssig, M. A. Green, Y. Lee, G. D. Samolyuk, P. Zajdel, J. W. Lynn, S. L. Bud'ko, M. S. Torikachvili, N. Ni, S. Nandi *et al.*, Pressure-induced volume-collapsed tetragonal phase of $CaFe_2As_2$ as seen via neutron scattering, Phys. Rev. B **78**, 184517 (2008).

[36] P. C. Canfield, S. L. Bud'ko, N. Ni, A. Kreyssig, A. I. Goldman, R. J. McQueeney, M. S. Torikachvili, D. N. Argyriou, G. Luke, and W. Yu, Structural, magnetic and superconducting phase transitions in $CaFe_2As_2$ under ambient and applied pressure, Phys. C: Supercond. Appl. **469**, 404 (2009).

[37] M. P. Smylie, K. Willa, J.-K. Bao, K. Ryan, Z. Islam, H. Claus, Y. Simsek, Z. Diao, A. Rydh, A. E. Koshelev *et al.*, Anisotropic superconductivity and magnetism in single-crystal $RbEuFe_4As_4$, Phys. Rev. B **98**, 104503 (2018).

[38] K. Jin, N. P. Butch, K. Kirshenbaum, J. Paglione, and R. L. Greene, Link between spin fluctuations and electron pairing in copper oxide superconductors, Nature (London) **476**, 73 (2011).

[39] R. A. Cooper, Y. Wang, B. Vignolle, O. J. Lipscombe, S. M. Hayden, Y. Tanabe, T. Adachi, Y. Koike, M. Nohara, H. Takagi *et al.*, Anomalous criticality in the electrical resistivity of $La_{2-x}Sr_xCuO_4$, Science **323**, 603 (2009).

[40] J. G. Analytis, H.-H. Kuo, R. D. McDonald, M. Wartenbe, P. M. C. Rourke, N. E. Hussey, and I. R. Fisher, Transport near a quantum critical point in $BaFe_2(As_{1-x}P_x)_2$, Nat. Phys. **10**, 194 (2014).

[41] S. Jiang, H. Xing, G. F. Xuan, C. Wang, Z. Ren, C. M. Feng, J. H. Dai, Z. A. Xu, and G. H. Cao, Superconductivity up to 30 K in the vicinity of the quantum critical point in $BaFe_2(As_{1-x}P_x)_2$, J. Phys.: Condens. Matter **21**, 382203 (2009).

[42] Y. Nakajima, R. X. Wang, T. Metz, X. F. Wang, L. M. Wang, H. Cynn, S. T. Weir, J. R. Jeffries, and J. Paglione, High-temperature superconductivity stabilized by electron-hole interband coupling in collapsed tetragonal phase of KFe_2As_2 under high pressure, Phys. Rev. B **91**, 060508(R) (2015).

[43] R. L. Stillwell, X. F. Wang, L. M. Wang, D. J. Campbell, J. Paglione, S. T. Weir, Y. K. Vohra, and J. R. Jeffries, Observation of two collapsed phases in $CaRbFe_4As_4$, Phys. Rev. B **100**, 045152 (2019).

[44] J. P. Sun, K. Matsuura, G. Z. Ye, Y. Mizukami, M. Shimozawa, K. Matsubayashi, M. Yamashita, T. Watashige, S. Kasahara, Y. Matsuda *et al.*, Dome-shaped magnetic order competing with high-temperature superconductivity at high pressures in FeSe, Nat. Commun. **7**, 12146 (2016).

[45] P. Dai, J. Hu, and E. Dagotto, Magnetism and its microscopic origin in iron-based high-temperature superconductors, Nat. Phys. **8**, 709 (2012).

[46] L. Fang, H. Q. Luo, P. Cheng, Z. S. Wang, Y. Jia, G. Mu, B. Shen, I. I. Mazin, L. Shan, C. Ren *et al.*, Roles of multiband effects and electron-hole asymmetry in the superconductivity and normal-state properties of $Ba(Fe_{1-x}Co_x)_2As_2$, Phys. Rev. B **80**, 140508(R) (2009).

[47] N. Doiron-Leyraud, P. Auban-Senzier, S. R. de Cotret, C. Bourbonnais, D. Jérome, K. Bechgaard, and L. Taillefer, Correlation between linear resistivity and T_c in the Bechgaard salts and the pnictide superconductor $Ba(Fe_{1-x}Co_x)_2As_2$, Phys. Rev. B **80**, 214531 (2009).

[48] P. C. Canfield, S. L. Bud'ko, N. Ni, J. Q. Yan, and A. Kracher, Decoupling of the superconducting and magnetic/structural phase transitions in electron-doped $BaFe_2As_2$, Phys. Rev. B **80**, 060501(R) (2009).

[49] F. Rullier-Albenque, D. Colson, A. Forget, and H. Alloul, Hall effect and resistivity study of the magnetic transition, carrier content, and Fermi-liquid behavior in $Ba(Fe_{1-x}Co_x)_2As_2$, Phys. Rev. Lett. **103**, 057001 (2009).

[50] T. Xie, Y. Wei, D. Gong, T. Fennell, U. Stuhr, R. Kajimoto, K. Ikeuchi, S. Li, J. Hu, and H. Luo, Odd and even modes of neutron spin resonance in the bilayer iron-based superconductor $CaKFe_4As_4$, Phys. Rev. Lett. **120**, 267003 (2018).

[51] Q. P. Ding, W. R. Meier, A. E. Bohmer, S. L. Budko, P. C. Canfield, and Y. Frukawa, NMR study of the new magnetic superconductor $CaK(Fe_{0.951}Ni_{0.049})_4As_4$: Microscopic coexistence of the hedgehog spin-vortex crystal and superconductivity, Phys. Rev. B **96**, 220510(R) (2017).

[52] J. Yuan, Q. H. Chen, K. Jiang, Z. P. Feng, Z. F. Lin, H. S. Yu, G. He, J. S. Zhang, X. Y. Jiang, X. Zhang *et al.*, Scaling of the strange-metal scattering in unconventional superconductors, Nature (London) **602**, 431 (2022).

[53] T. Shibauchi, A. Carrington, and Y. Matsuda, A quantum critical point lying beneath the superconducting dome in iron-pnictides, Annu. Rev. Condens. Matter Phys. **5**, 113 (2014).

[54] N. Barbero, S. Holenstein, T. Shang, Z. Shermadini, F. Lochner, I. Eremin, C. Wang, G. H. Cao, R. Khasanov, H. R. Ott *et al.*, Pressure effects on the electronic properties of the undoped superconductor ThFeAsN, Phys. Rev. B **97**, 140506(R) (2018).

[55] S. Sen and G.-Y. Guo, Pressure induced Lifshitz transition in ThFeAsN, Phys. Rev. Mater. **4**, 104802 (2020).

[56] F. Schrodi, F. C. Kabeer, A. Aperis, and P. M. Oppeneer, Exploring multichannel superconductivity in ThFeAsN, Phys. Rev. B **104**, 094516 (2021).